Chemosphere 290 (2022) 133298

Contents lists available at ScienceDirect

Chemosphere

journal homepage: www.elsevier.com/locate/chemosphere

The role of freshwater sludge and its carbonaceous derivatives in the removal of lead, phosphorus and antibiotic enrofloxacin: Sorption characteristics and performance

Yunhui Zhang [a,b,c], Olusegun K. Abass [b], Junde Qin [b], Yaolin Yi [b,*]

[a] Key Laboratory of Yangtze River Water Environment, Ministry of Education, College of Environmental Science and Engineering, Tongji University, Shanghai, 200092, China
[b] School of Civil and Environmental Engineering, Nanyang Technological University, 639798, Singapore
[c] Shanghai Institute of Pollution Control and Ecological Security, Shanghai, 200092, China

HIGHLIGHTS

- Remove Pb, P and ENR with FS and derived biochar and hydrochar.
- Adsorption capacity for Pb follows order of biochar > FS > hydrochar.
- Adsorption capacity for P follows order of FS > biochar > hydrochar.
- ENR adsorption follows BET isotherm model, dominated by physical adsorption.
- Adsorption on all adsorbents was affected by solution pH.

GRAPHICAL ABSTRACT

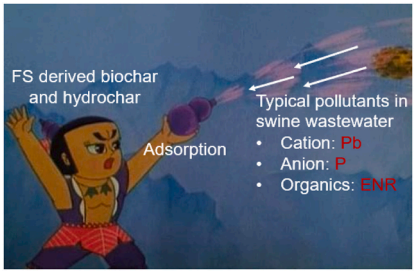

ARTICLE INFO

Handling Editor: Lei Wang

Keywords:
Sludge
Biochar
Hydrochar
Sorption
Antibiotics
Phosphorous

ABSTRACT

Freshwater sludge (FS) produced from drinking water treatment plants is generally filter pressed and disposed in the landfill. However, FS could be potentially reused. In this study, FS were processed into biochar and hydrochar via pyrolysis and hydrothermal carbonization, respectively. The sorption characteristics/mechanisms of FS and its derivatives (biochar-B300, B500 and B700 and hydrochar-H140, H160, H180 and H200) for the removal of three typical pollutants (i.e., lead (Pb), phosphorus (P) and enrofloxacin (ENR)) found in swine wastewater were investigated using batch adsorption tests and microstructural analyses. It was found that Pb sorption was relatively enhanced due to the increased electrostatic attraction and surface precipitation of $Pb(OH)_2$ while the anionic phosphate adsorption relatively decreased as a result of enhanced electrostatic repulsion at higher solution pHs. Comparatively, ENR adsorption was less affected by solution pH probably due to dominance of physical adsorption evidenced by the good fitting of the BET isotherm model ($R^2 = 0.95$). The maximum sorption capacities of Pb were in the order of B700≈B500 (71 mg/g)>B300 ~ FS(37 mg/g)>H140 ~ H160 (13 mg/g)> H180 ~ H200 (6 mg/g). The adsorption capacities for P were relatively lower: FS (47 mg/g)>B300 (38 mg/g)> H140 (27 mg/g)>B700 (37 mg/g)≈B500 (24 mg/g)≈H160 (23 mg/g)>H180 (16 mg/g)>H200 (14 mg/g). This study provides an understanding of the sorption characteristics and mechanisms of FS and its carbonaceous products for common cationic, anionic and organic pollutants and elucidates new insights into the reuse of FS for

* Corresponding author.
E-mail address: yiyaolin@ntu.edu.sg (Y. Yi).

https://doi.org/10.1016/j.chemosphere.2021.133298
Received 23 September 2021; Received in revised form 22 November 2021; Accepted 11 December 2021
Available online 16 December 2021

pollutant removal to achieve the waste-to-resource concept and enhance water quality, soil health and food safety.

1. Introduction

It is undoubted that the environmental pollution is increasingly severe due to the continuous increase in the amount and types of pollutants brought by intense human activities (Xu et al., 2019). The accelerated rate of production of raw sewage from swine-breeding facilities in many countries, such as China, have become an increasing cause of concern due to the accumulation of heavy metals and antibiotics present in them, which poses great environmental threat even at trace levels. Heavy metals are characteristically of high toxicity and are persistent in the environment (Zhang et al., 2019). In swine-breeding facilities, they are usually administered to the animals as integrators in conjunction with antibiotics and the raw sewage discharge can have toxic effects on plants and organisms present in the various environmental compartments (including soil and water) by obstructing the metabolic functions and upsetting the balance in the normal ion absorption, transport, and regulation pathways (Wu et al., 2011). Similarly, the persistence of antibiotics in the environment can lead to the prevalence of resistant bacterial strains. For instance, fluoroquinolone such as enrofloxacin are excreted largely unchanged (<25% metabolized) and can enter the environment via discharge of raw or untreated swine-breeding wastewater onto agricultural soils as fertilizers (Golet et al., 2002). Although phosphorus is a vital element for vegetation growth, its excessive release is mainly responsible for eutrophication, largely reducing the level of dissolved oxygen in the water and the quality of aquatic ecosystems. These pollutants are generally present in swine wastewater and recent data shows that swine breeding in China occupies approximately 63% of the total meat production (Fan et al., 2019a). According to empirical statistics, the rate of production of breeding waste per 10,000 pigs have reached approximately 190 t/d with 60% of the waste being swine effluent/wastewater (Fan et al., 2019b, 2021). Therefore, an efficient and cost-effective process that is targeted at eliminating the toxic and harmful chemical pollutants in such wastewater are urgently required.

Extensive efforts have targeted the removal of these pollutants, including biological reduction, advanced oxidation processes, precipitation, reverse osmosis, co-composting and adsorption (Shen et al., 2018; Chowdhury et al., 2019; Fan et al., 2021; Liu et al., 2021). Adsorption is one of the most cost-effective and efficient ways to remove these pollutants (Liu et al., 2021; Zhang et al., 2021a) and carbonaceous materials, such as biochar and hydrochar, have gained great attention in the academia and industrial field due to their low costs, carbon storage and sustainability (Nzediegwu et al., 2021; Pauletto et al., 2021). However, only few studies compared the adsorption performance and characteristics of biochar and hydrochar with the same feedstock to remove pollutants in aqueous solutions. Chen et al. (2021) compared the adsorption and reduction of Cr(VI) on fallen leaves derived biochar and hydrochar and found that hydrochar with more surface phenolic groups can chemically complex with Cr(VI) and are able to sustain higher Cr(VI) adsorption and photo-reduction ability. Zhang et al. (2020) produced spent coffee grounds-based biochar and hydrochar and used them to adsorb antibiotic sulfonamide. The results showed that the adsorption capacity of biochar was higher than that of hydrochar. In addition, the adsorption on biochar was dominated by π-π electron donor-acceptor interactions while hydrogen bonds took an important part in the adsorption on hydrochar. The inconsistent findings for adsorbent characteristics are mainly attributed to different pollutants, feedstock, and production conditions of carbonaceous materials used in the different studies, causing difficulty and inaccuracy in the comparison. Therefore, it is crucial to comprehensively compare the sorption characteristics of biochar and hydrochar derived from the same material for different kinds of pollutants found in swine wastewater, such as cationic metal ions, anionic inorganic salts and recalcitrant organics to find out the structure-function relationship of carbonaceous products derived from the same feedstock for sorption and further guide the recycling of waste materials and their practical applications in pollution control.

Freshwater sludge (FS) is a by-product from drinking water treatment plants and its global production is estimated to be more than 10,000 t/day (Turner et al., 2019). Currently, FS in Singapore is sent to landfill for disposal as sludge cake to reduce its impact on the environment. However, FS is a potential useful resource. Some studies have focused on its reutilization as soil amendments, building and construction materials, adsorbents or coagulants, etc (Babatunde and Zhao, 2007; Dassanayake et al., 2015; Mazari et al., 2018). However, the natural organic matter, organic pollutants, metals and microorganisms likely existing in FS (Babatunde and Zhao, 2007) can reduce its effectiveness and limits its application in these fields. Therefore, the removal of organic matters and microorganisms have been conducted using calcination (Jeon et al., 2018), pyrolysis and hydrothermal carbonization (Zhang et al., 2021b). Zhang et al. (2021b) produced and characterized FS derived biochar and hydrochar at different temperatures and the results indicated that the produced chars hold a huge potential as adsorbents due to their high surface areas and low metal levels. However, to the best of the authors' knowledge, the sorption performance of FS-derived carbonaceous products has not been reported and compared in previous studies.

Thus, this study aims to assess the sorption effectiveness of three model pollutants in swine wastewater (i.e., lead, phosphorus and enrofloxacin) on FS produced in Singapore and its derived carbonaceous materials. The objectives are (1) to calculate and compare sorption capacities of Pb, P and ENR on FS and derived biochar and hydrochar produced at different temperatures; (2) to assess the effects of pH on their sorption performance; and (3) to explore their sorption mechanisms. This study is expected to provide new insights into the reuse of FS for pollutant removal to achieve the waste-to-resource concept.

2. Materials and methods

2.1. Materials and synthesis of FS derivatives

The dewatered FS was freeze-dried for 48 h and sieved to smaller than 75 μm. The production and properties of biochar and hydrochar samples can be found in Zhang et al. (2021b). Briefly, biochar samples were prepared by the pyrolysis of FS at 300, 500 and 700 °C for 1 h at a heating rate of 10 °C/min under the N_2 environment in a horizontal rotary reactor, and were labeled as B300, B500 and B700. Hydrochar samples were produced by hydrothermal carbonization of freeze-dried FS at 140, 160, 180 and 200 °C for 4 h under autogenous pressure in an autoclave (4744 General purpose acid digestion vessel, Parr Instrument Company). The produced hydrochar samples were dried at 60 °C for 24 h before sieved below 75 μm and were labeled as H140, H160, H180 and H200. $Pb(NO_3)_2$, NaH_2PO_4, $NaNO_3$, NaCl and ENR used in this study are A.R. grade.

2.2. Determination of point of zero charge

The determination of the point of zero charge (pHpzc) of FS and char samples was conducted using the pH drift method (Qu et al., 2020). A solution containing 0.01 M NaCl was bubbled with nitrogen gas for several minutes to remove the dissolved CO_2. Then, the solution pH was adjusted between 2 and 11 using NaOH or HCl solution. 0.15 g of solid sample was added into 50 mL NaCl solution, and the final pH of the

Table 1
Physiochemical properties of FS and derived biochar and hydrochar.

	pH_{PZC}	pH	Surface area (m^2/g)
FS	6.11	6.57	96.50
B300	4.68	4.91	104.67
B500	7.03	7.63	109.85
B700	7.74	7.78	108.87
H140	4.26	4.49	156.91
H160	4.07	4.50	230.70
H180	4.02	4.42	285.78
H200	3.88	4.32	197.61

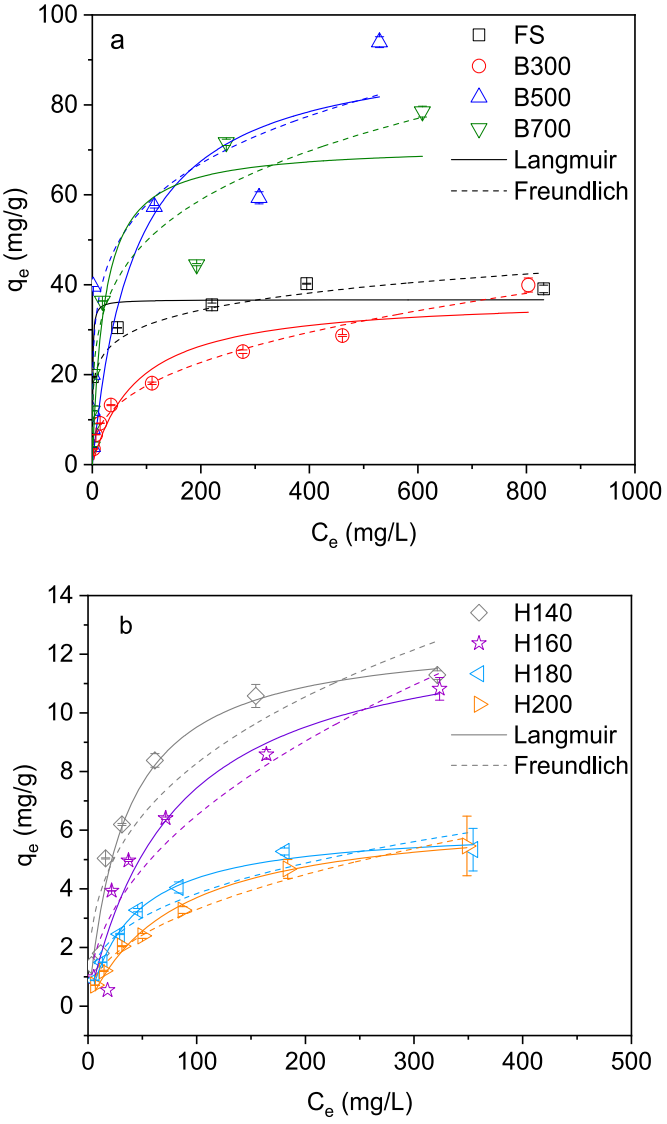

Fig. 1. Sorption isotherms of Pb on FS and derived biochar (a) and hydrochar (b).

filtrate was measured after 48 h of shaking at 200 rpm at room temperature. The pHpzc is defined as the point where $pH_{final} = pH_{initial}$.

2.3. Batch sorption experiments

2.3.1. Sorption isotherms

Solutions with different Pb^{2+} concentrations (20.7, 41.4, 62.1, 103.5, 207, 414, 621 and 1035 mg/L) and 0.01 M $NaNO_3$ were applied to explore the sorption isotherm. It should be noted that compared with Pb, Zn, Mn, and Cu are the most abundant heavy metals in swine wastewater and previous studies have discussed their removal or recovery (Chu et al., 2018; Li et al., 2020a, 2020b). However, studies on the removal of Pb in swine wastewater are limited. Thus, Pb was chosen for removal in conjunction with other common pollutants in swine wastewater. As for the P adsorption, the $H_2PO_4^-$ concentrations are set at 25, 50, 100, 200, 400 and 800 mgP/L. The ENR adsorption was conducted by adjusting a series of ENR concentrations (10, 20, 40, 60, 80 and 100 mg/L). The liquid/solid ratio was 0.1 g/20 mL, and the initial solution pH was adjusted at 5 using 0.1 M HNO_3 and 0.1 M NaOH. The mixtures were filtered using a 0.45 μm filter after shaking for 24 h. Pb and P concentrations were determined by inductively coupled plasma/optical emission spectrometry (ICP-OES) (PerkinElmer, 7000DV) after dilution and acidification, and ENR concentrations were measured using High-Performance Liquid Chromatography (HPLC) (PerkinElmer, Flexar). The detection limits of ICP-OES for Pb and P are 0.1 mg/L and that of HPLC for ENR is 2 mg/L, respectively.

2.3.2. Effect of the solution pH

The influence of pH was evaluated by the addition of 0.1 g of solid sample to 20 mL of 207 mgPb/L $Pb(NO_3)_2$ solution (containing 0.01 M $NaNO_3$), 100 mgP/L NaH_2PO_4 solution or 60 mg/L ENR solution. The pH range of real swine wastewater modeled is between 7.52 and 7.56 (Fan et al., 2021). However, based on the acid-base properties of adsorbates, the sorption is strongly dependent on pH. Thus, the initial solution pH in the range of 4–8 were evaluated. The mixtures were filtered before pollutants concentration measurement.

2.4. Microstructural analysis

The functional groups were tested by Fourier transform infrared spectroscopy (FTIR) spectrometer in the wavelength range of 600–4000 cm^{-1} by 32 scans at 4 cm^{-1} resolution (PerkinElmer Frontier) before and after Pb and P sorption for each sample. Thermogravimetric analyses were carried out using a Thermogravimetric Analyzer TGA 4000 (PerkinElmer). The sample was heated from 30 °C at 10 °C/min until 900 °C in an air atmosphere using a flow rate of 20 mL/min.

3. Results and discussion

3.1. Physicochemical properties of FS and derived chars

Table 1 lists some physicochemical properties of FS and derived biochar and hydrochar. The point of zero charge (pH_{PZC}) values were measured in this study, and other characteristics were previously investigated in (Zhang et al., 2021b). The point of zero charge (pH_{PZC}) of adsorbents is an important influencing factor for the sorption of cations and anions, such as Pb and P, by changing the surface charge of adsorbents (Shen et al., 2015). If the solution pH is above pH_{PZC}, the solid surface of sorbents is negatively charged and holds a higher affinity to sorb cations, such as Pb^{2+}, but a lower adsorption ability to anions, such as phosphate species and vice versa (Zhang et al., 2021a). The pH_{PZC} values of FS, B300, B500, B700, H140, H160, H180 and H200 were measured at 6.11, 4.68, 7.03, 7.74, 4.26, 4.07, 4.02 and 3.88, respectively. The sorption of Pb and P at different pHs will be further discussed in sections 3.2 and 3.3. In addition, the sorbents with a higher surface area, such as H160 and H180, are more likely to have more adsorption sites which is favorable for adsorption.

3.2. Pb sorption characteristics

Equilibrium sorption of heavy metals and phosphate onto char samples is often fast and occurs within 12 h (Zou et al., 2006; Karatas, 2012). Therefore, sorption kinetics were not conducted and the sorption tests lasted for 24 h in this study to ensure sorption equilibrium has been reached. The sorption isotherms of Pb on FS and derived chars are

Table 2
Isotherm model parameters for Pb sorption on FS and derived biochar and hydrochar.

	Langmuir				Freundlich			
	Q_0 (mg/g)	b (L/mg)	AIC	R^2	K_F (mg/g)	1/n	AIC	R^2
FS	36.68 ± 3.51	1.33 ± 0.86	40.67	0.81	15.47 ± 4.59	0.15 ± 0.05	41.65	0.78
B300	37.39 ± 4.47	0.012 ± 0.005	32.83	0.90	3.16 ± 0.42	0.37 ± 0.02	15.52	0.99
B500	71.01 ± 9.21	0.68 ± 0.58	53.70	0.79	21.76 ± 10.01	0.21 ± 0.08	52.89	0.81
B700	71.04 ± 10.84	0.05 ± 0.04	51.78	0.80	16.18 ± 10.38	0.24 ± 0.11	50.02	0.84
H140	12.72 ± 0.88	0.03 ± 0.01	3.19	0.96	1.66 ± 0.55	0.35 ± 0.07	10.79	0.86
H160	13.22 ± 1.81	0.013 ± 0.004	5.52	0.92	0.73 ± 0.32	0.47 ± 0.09	8.44	0.88
H180	6.14 ± 0.18	0.025 ± 0.002	0.12	0.99	0.78 ± 0.21	0.35 ± 0.05	1.49	0.90
H200	6.64 ± 0.31	0.013 ± 0.002	0.17	0.99	0.43 ± 0.07	0.44 ± 0.03	0.36	0.98

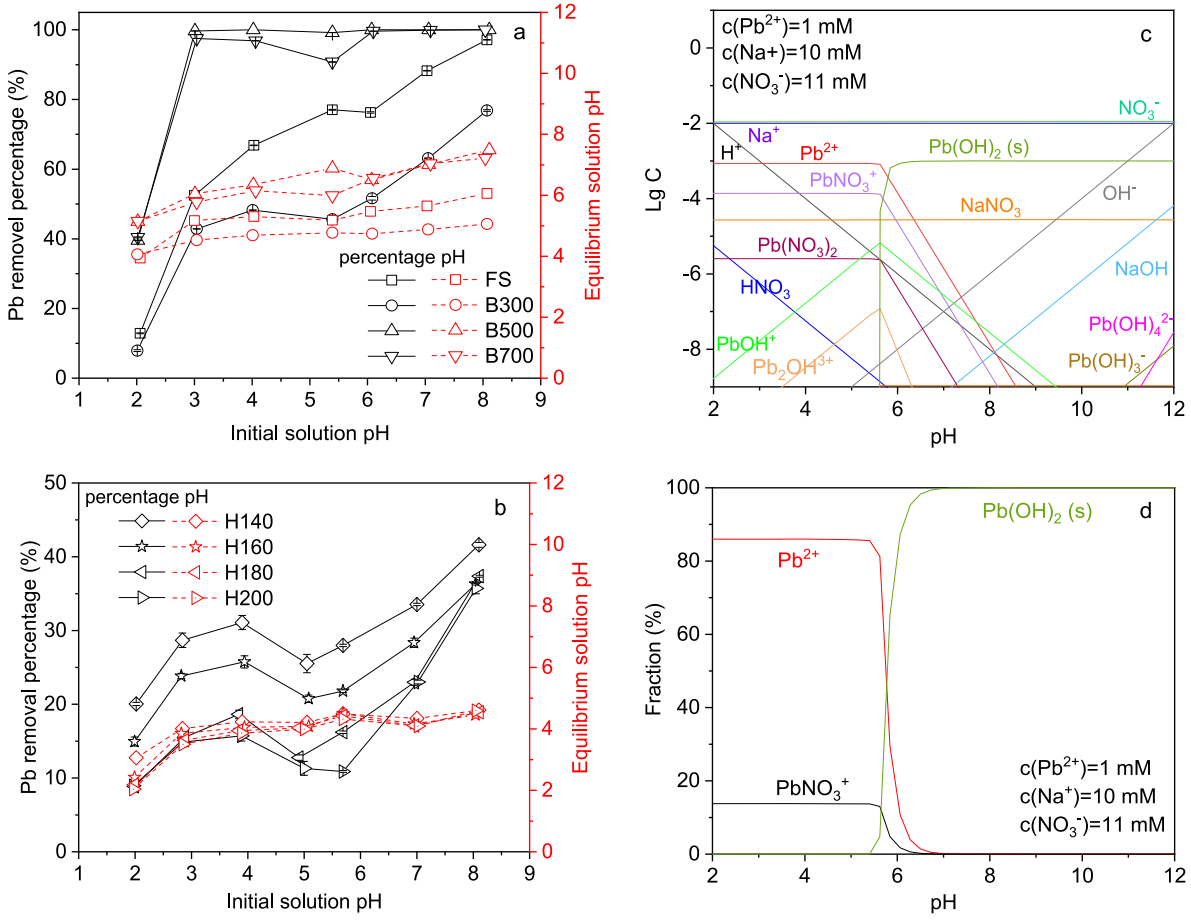

Fig. 2. Effect of initial solution pH on the percentage of Pb(II) removal on FS and derived biochar (a) and hydrochar (b), and speciation diagrams for all species (c) and Pb species (d).

shown in Fig. 1. Langmuir and Freundlich models (Table S1) were applied to fit the experimental data and can both describe the Pb sorption with the R^2 value higher than 0.78. However, to be specific, the Pb sorption on FS and hydrochar was described better by the Langmuir model while that on biochar fit the Freundlich model due to higher R^2 value and lower AIC value (Table 2). This indicates that the Pb sorption on FS and hydrochar was a monolayer surface adsorption and that on biochar was a heterogeneous process in which Pb was mainly sorbed on the heterogeneous surface pore structure and functional groups of biochar. The maximum sorption capacity (Q_0) was in the order of B700 ~ B500 (~71 mg/g) >B300 ~ FS (~37 mg/g) >H140 ~ H160 (~13 mg/g) > H180 ~ H200 (~6 mg/g). That is, the adsorption capacity of biochar decreased with pyrolysis temperature but higher than that of an anaerobic digestion sludge biochar (49.93 mg/g) (Ho et al., 2017) and a sewage sludge biochar (30.88 mg/g) (Lu et al., 2012).

Solution pH is an important parameter for metals sorption and the effect of pH on Pb sorption is shown in Fig. 2. Unsurprisingly, the Pb removal showed an overall increasing trend with the increase in initial solution pH from 2 to 8 in spite of a temporary decrease at pH 4–5 for hydrochar samples. The increase in Pb removal when pH was above 5 is mainly attributed to the precipitation of Pb^{2+} according to the speciation diagrams modeled by the Medusa software (Zhang et al., 2018) under the conditions of this study (Fig. 2c and d). The increase in Pb adsorption in the acidic pH range can be explained by the increase in negative sites created by the deprotonation process of functional groups on the sorbent surface (Shen et al., 2017). With the increasing initial

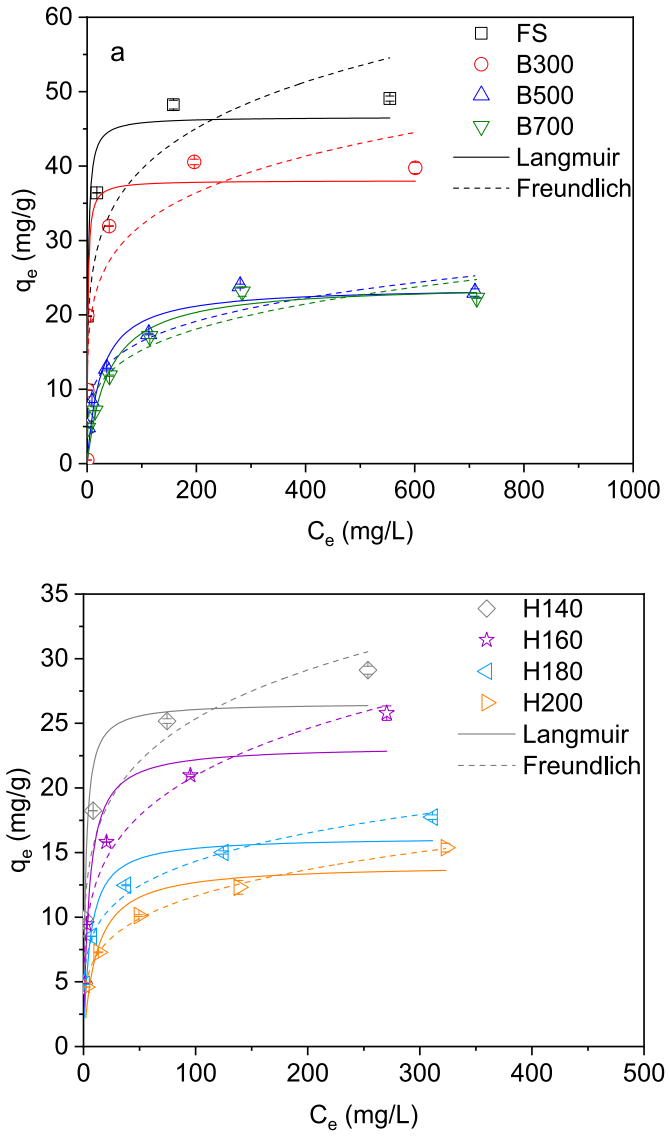

Fig. 3. Adsorption isotherms of P on FS and derived biochar (a) and hydrochar (b).

solution pH from 2 to 8, the equilibrium pH increased slightly in the range of pH 2–3 and then kept constant at pH values similar to their pHpzc as listed in Table 1. This shows the good buffering ability of FS and derived char samples under a wide range of pH, and indicates a possible resistance to changing pH in aqueous solutions, which is beneficial for their practical applications for metals removal. However, hydrochar samples performed less competitively to the biochar samples considering their overall lower Pb removal percentage and decreasing Pb removal in the pH range of 5–6 which fall within the common pH range of natural water bodies.

To further figure out the possible Pb sorption mechanisms on the sorbents, various spectroscopic analyses, including FTIR (Fig. S1) and TGA (Fig. S2), were performed before and after sorption. As shown in both figures, the broad band at around 3445 cm^{-1} reflected the stretching vibrations of hydroxyl groups (—OH) connected to metal ions or sorbed water molecules (Li et al., 2016). The peak at around 1300 cm^{-1} is attributed to CO_3^{2-}, which appeared after Pb sorption on B500 and B700 samples, indicating the formation of $PbCO_3$ which may explain the higher sorption capacity of these two samples. The FTIR spectra in Fig. S1b did not show obvious changes after Pb sorption on hydrochar samples, indicating that the functional groups on the hydrochar surface have little interactions with Pb^{2+}, consistent with their low sorption capacity.

The TGA/DTG curves of FS and derived char samples before and after Pb sorption are presented in Fig. S2. The total weight loss of biochar after Pb sorption increased compared to the initial weight value before Pb sorption while in the case of FS and hydrochar, there was no observable difference between the weight value before and after Pb sorption. The sharp peak at around 100 °C in the DTG patterns in Figs. S2c and S2d indicates dehydration and the new peak at about 350 °C for samples after Pb sorption is probably attributed to the formation of $PbCO_3$ which is in agreement with the FTIR findings. Based on the above microstructural analyses, the formation of $PbCO_3$ is one of the Pb sorption mechanisms on the surface of FS and derived char samples, especially for FS and hydrochar samples.

3.3. P adsorption characteristics

Langmuir and Freundlich isotherm models were used to fit the experimental data for P adsorption as shown in Fig. 3 and Table 3. Both models can describe the adsorption isotherm well with R^2 values higher than 0.80, although the Langmuir model fits the P adsorption on FS and biochar better and that on hydrochar is better fit by the Freundlich model based on higher R^2 values and lower AIC values. That is, P adsorption on FS and biochar tends to be the monolayer surface adsorption while that on hydrochar was heterogeneous. According to the Langmuir model, the adsorption capacity for P showed different order compared with Pb with much lower values on the whole: FS (~47 mg/g) >B300 (~38 mg/g) >H140 (~27 mg/g) >B700 (~37 mg/g)≈ B500 (~24 mg/g)≈H160 (~23 mg/g) >H180 (~16 mg/g) >H200 (~14 mg/g). The adsorption capacities are extremely higher than that of a sludge-derived biochar (0.25 mg/g) (Li et al., 2020a, 2020b) and are comparable with a dolomite-modified sewage sludge derived biochar (29.18 mg/g) (Li et al., 2019). The lower P adsorption capacity is related to the negative sample surface, which inhibits the adsorption of P in anionic forms ($H_2PO_4^-$, HPO_4^{2-} and PO_4^{3-}) as shown in Fig. 4c and d. In addition, $H_2PO_4^-$ species was dominant at acidic pH and the phosphate with more negative charges (HPO_4^{2-} and PO_4^{3-}) gradually became the main species with the increase in solution pH. This is also the rationale behind the decrease in P adsorption with increasing pH as shown in

Table 3
Isotherm model parameters for P adsorption on FS and its derived biochar and hydrochar.

	Langmuir				Freundlich			
	Q_0 (mg/g)	b (L/mg)	AIC	R^2	K_F (mg/g)	1/n	AIC	R^2
FS	46.61 ± 3.42	0.57 ± 0.22	35.87	0.94	16.72 ± 4.02	0.19 ± 0.05	40.36	0.87
B300	38.06 ± 4.19	0.76 ± 0.44	38.96	0.85	13.86 ± 4.22	0.18 ± 0.06	40.51	0.81
B500	23.83 ± 2.39	0.04 ± 0.02	28.39	0.89	6.01 ± 1.20	0.22 ± 0.04	24.73	0.94
B700	24.25 ± 2.23	0.03 ± 0.01	26.10	0.92	4.90 ± 1.30	0.25 ± 0.05	26.57	0.92
H140	26.58 ± 2.23	0.50 ± 0.24	39.06	0.93	10.08 ± 1.76	0.20 ± 0.04	38.52	0.93
H160	23.25 ± 2.15	0.21 ± 0.104	38.02	0.91	7.24 ± 0.75	0.23 ± 0.02	29.85	0.98
H180	16.21 ± 1.51	0.17 ± 0.09	34.72	0.88	5.58 ± 0.40	0.20 ± 0.02	22.68	0.99
H200	14.09 ± 1.60	0.09 ± 0.05	34.15	0.84	3.96 ± 0.14	0.23 ± 0.01	11.96	1.00

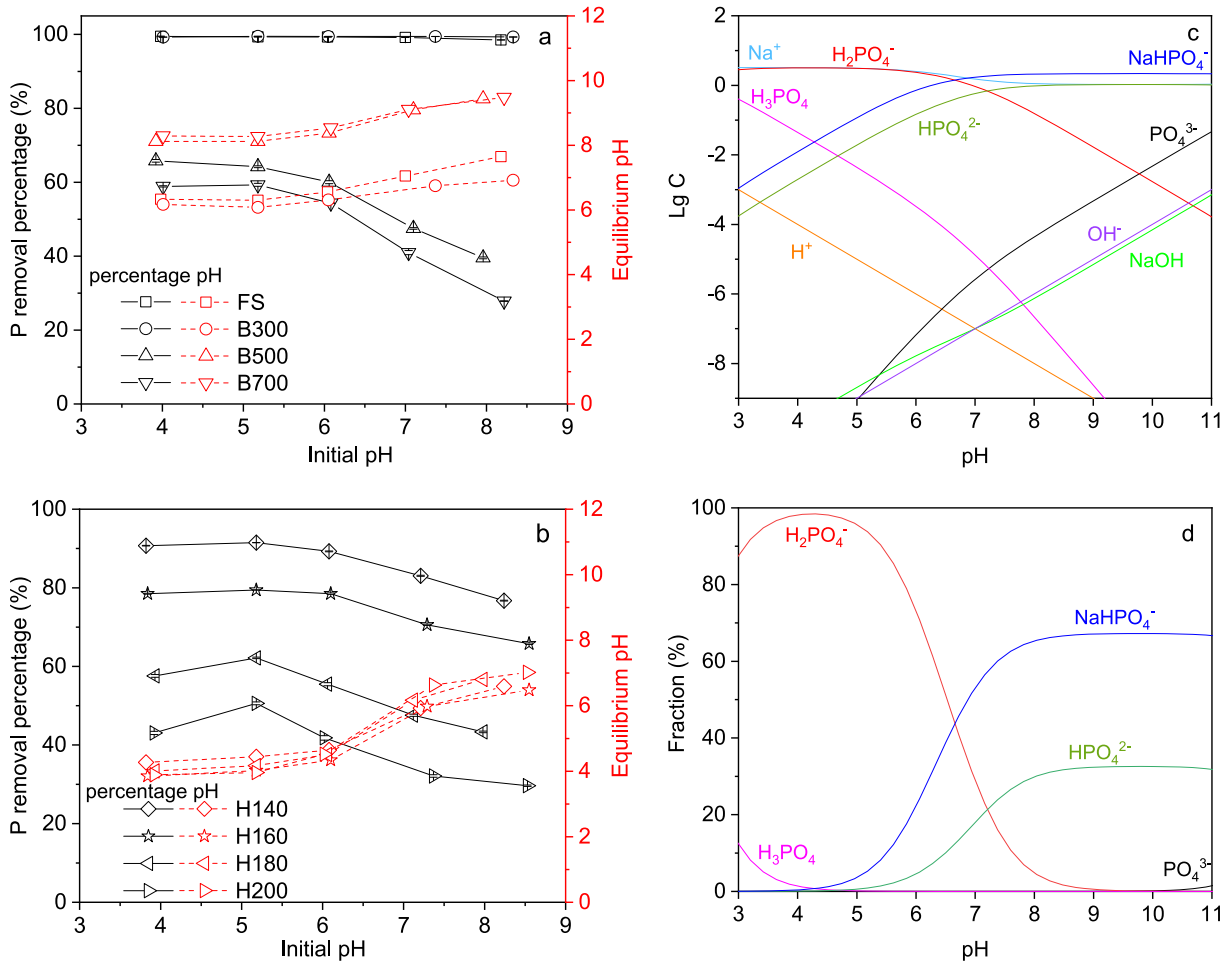

Fig. 4. Effect of initial solution pH on the percentage of P removal on FS and derived biochar (a) and hydrochar (b), and speciation diagrams for all species (c) and P species (d).

Fig. 4a and b, indicative of enhanced electrostatic repulsion. The solution pH after adsorption decreased and the increasing trend of hydrochar adsorption systems was more obvious. The same phenomenon was also shown in Fig. 1 in terms of Pb sorption. This can be explained by the acidic pH of hydrochar as shown in Table 1, and the acidic hydrochar can decrease the solution pH.

FTIR spectra in Fig. S3 show the changes of functional groups on the adsorbent surface before and after P adsorption. The clear peak at around 1037 cm^{-1} is attributed to the asymmetric P–O stretching vibration (Lee et al., 2019; Dong et al., 2020). The increased peak intensities after P adsorption imply the adsorption of phosphate on adsorbents, and the intensity changes were found consistent with the phosphorous adsorption capacities in Table 2 in the order of FS > biochar > hydrochar. The higher peak intensity at 1380 cm^{-1} is likely due to the stretching vibration of nitrate (Zhang et al., 2013) which was used to adjust ionic strength in this study.

3.4. ENR adsorption characteristics

As shown in Fig. 5, the adsorption isotherms of ENR on FS and derived adsorbents were fitted by the Langmuir, Freundlich and modified form of BET model (Table S1) with isotherm equations, parameters and regression analysis presented in Table 4. The BET model can well describe the ENR adsorption on adsorbents in this study with the R^2 values higher than 0.95, indicating multilayer physical adsorption processes. However, the Freundlich model can better fit the ENR adsorption on hydrochar considering the lower AIC values and standard deviation. In the BET model, K_B and K_L are the equilibrium constants of adsorption on the first and upper layers, respectively. Therefore, the ENR adsorption on the first layer was at least 10 times quicker than that on the second layer for all adsorbents.

Compared to the adsorption of Pb and P, the ENR adsorption on FS, biochar and hydrochar is more resistant to the change of solution pH despite the slight increase in the removal percentage with increasing solution pH. This can be probably explained by the inference from the best fitting of the BET isotherm model that the ENR adsorption was dominated by physical adsorption which is not significantly affected by solution pH. These findings are also supported by the FTIR spectra (Fig. S4) showing negligible changes in the surface functional groups before and after ENR adsorption. The slight variation of ENR removal at different pHs is probably due to existing forms of ENR at different pHs. As shown in Fig. 6c, ENR exists in the cationic form at acidic conditions, becomes zwitterionic gradually in the pH range of 6–8.5, and the anionic ENR species dominate at pH higher than 8.5. The low removal percentage of B700 at acidic pH in the presence of cationic ENR species can be probably explained by the positively charged surface of B700 with the highest pH_{PZC} value (7.74) as shown in Table 1. The highest ENR removal occurred at pH > 7 for all adsorbents, which is likely due to the enhanced hydrophobic interaction between the slightly hydrophobic surface of the adsorbents and hydrophobic zwitterionic ENR species at pH 6–8 (Zhao et al., 2018).

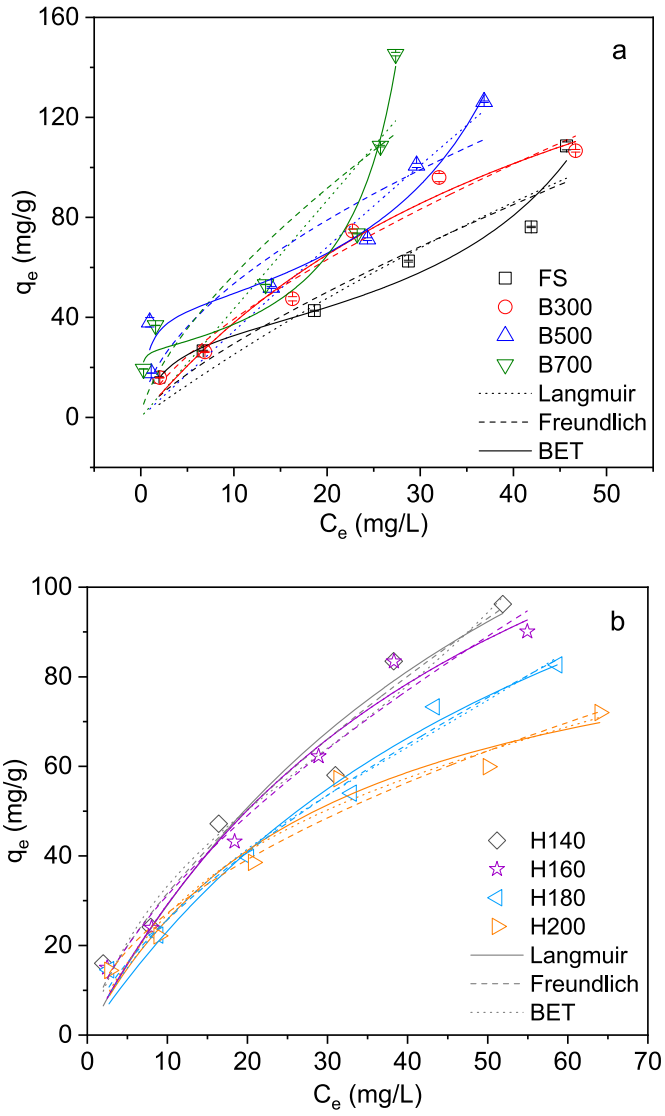

Fig. 5. Adsorption isotherms of ENR on FS and derived biochar (a) and hydrochar (b).

Table 4
Isotherm model parameters for ENR adsorption on FS and derived biochar and hydrochar.

Models	Parameters	FS	B300	B500	B700	H140	H160	H180	H200
Langmuir	Q_0 (mg/g)	444.12 ± 692.22	230.57 ± 61.26	2497.01 ± 29196.19	–	202.78 ± 77.02	179.73 ± 40.10	174.67 ± 45.24	101.88 ± 14.60
	b (L/mg)	0.006 ± 0.01	0.020 ± 0.009	0.001 ± 0.017	–	0.017 ± 0.010	0.019 ± 0.007	0.015 ± 0.007	0.034 ± 0.011
	AIC	45.22	38.86	51.33	–	40.40	36.02	34.70	34.33
	R^2	0.90	0.97	0.81	–	0.95	0.98	0.97	0.97
Freundlich	K_F (mg/g)	5.08 ± 3.18	8.18 ± 2.50	14.71 ± 9.66	11.84 ± 14.00	6.76 ± 2.20	6.96 ± 1.85	5.52 ± 1.16	8.11 ± 1.95
	1/n	0.76 ± 0.17	0.68 ± 0.09	0.56 ± 0.20	0.68 ± 0.30	0.67 ± 0.09	0.65 ± 0.07	0.67 ± 0.06	0.53 ± 0.06
	AIC	44.14	39.78	50.02	54.63	38.06	36.00	31.01	33.82
	R^2	0.92	0.97	0.85	0.76	0.97	0.98	0.99	0.97
BET	q_m (mg/g)	33.67 ± 7.00	230.57 ± 946.64	42.46 ± 7.13	26.32 ± 4.88	59.55 ± 24.03	179.73 ± 530.79	65.80 ± 31.18	69.39 ± 41.05
	K_B (L/mg)	0.41 ± 0.42	0.02 ± 0.09	1.73 ± 1.68	16.12 ± 52.59	0.10 ± 0.09	0.02 ± 0.06	0.06 ± 0.05	0.06 ± 0.06
	K_L (L/mg)	0.015 ± 0.002	0	0.018 ± 0.002	0.030 ± 0.002	0.009 ± 0.004	0	0.006 ± 0.004	0.003 ± 0.005
	AIC	68.98	68.86	72.68	72.65	68.57	66.02	63.61	64.01
	R^2	0.97	0.97	0.96	0.97	0.96	0.98	0.98	0.97

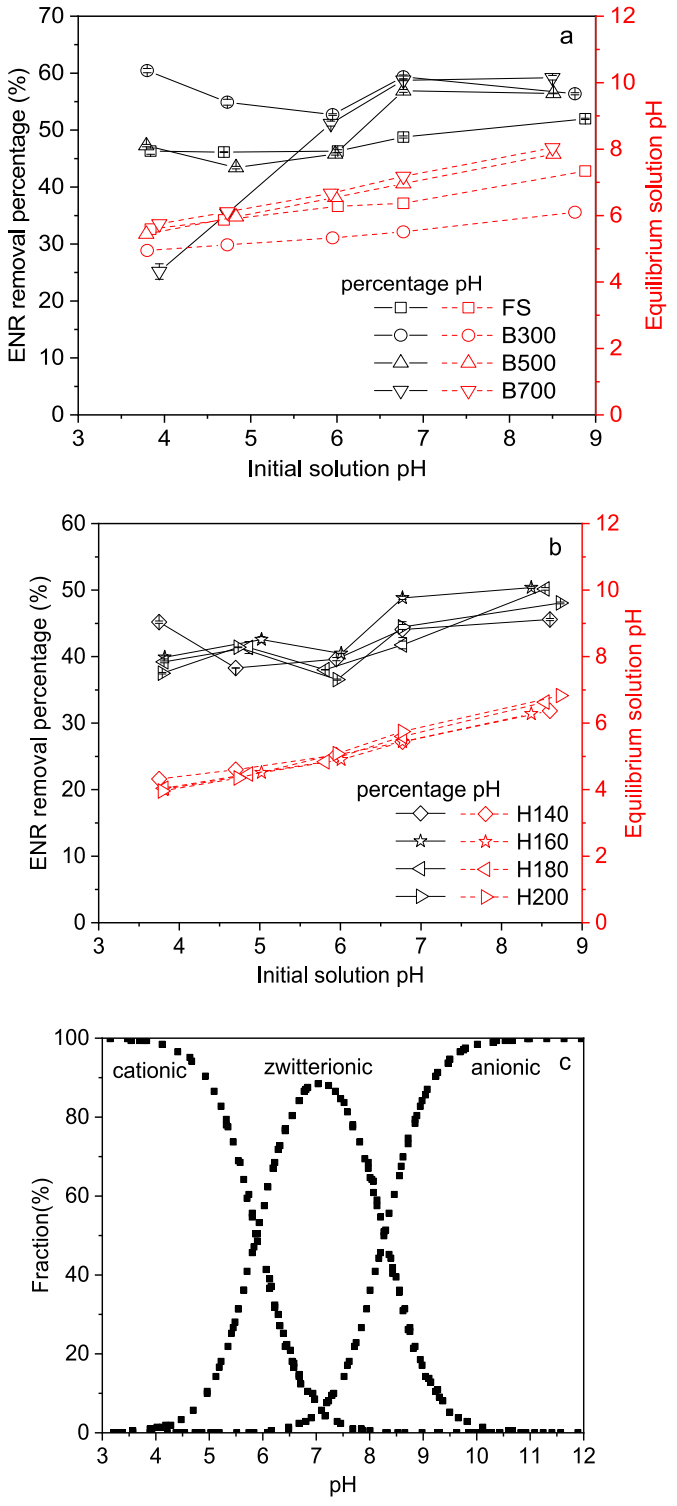

Fig. 6. Effect of initial solution pH on the percentage of ENR removal on FS and derived biochar (a) and hydrochar (b), and distribution of ENR species (c) (Zhao et al., 2018).

4. Conclusions

In this study, the sorption of three typical swine wastewater pollutants (Pb, P and ENR) on freshwater sludge and derived biochar and hydrochar were investigated. The following conclusions could be drawn:

(1) Pb sorption on FS and hydrochar was found a monolayer surface adsorption while its adsorption on biochar was a heterogeneous process. The sorption mechanisms include the surface precipitation of $PbCO_3$ and $Pb(OH)_2$ and electrostatic attraction.
(2) P adsorption was found a monolayer surface adsorption process on FS and biochar but a heterogeneous process on hydrochar with the adsorption capacity in the order of FS > biochar > hydrochar.
(3) The ENR adsorption on FS and carbonaceous products was most likely dominated by physical adsorption evidenced by the good fitting of the BET isotherm model although the Freundlich model could better fit its adsorption on hydrochar.
(4) The sorption of three pollutants on FS and carbonaceous products was affected by the solution pH, indicating the significant role of electrostatic attraction in the adsorption.

Credit author statement

Yunhui Zhang: Methodology, Investigation, Data curation, Writing-Original draft preparation. **Olusegun K. Abass:** Investigation, Data curation, Funding acquisition (ENR part), Reviewing and Editing. **Junde Qin:** Investigation, Data curation. **Yaolin Yi:** Conceptualization, Methodology, Funding acquisition, Writing- Reviewing and Editing.

Declaration of competing interest

The authors declare that they have no known competing financial interests or personal relationships that could have appeared to influence the work reported in this paper.

Acknowledgments

The authors would like to thank Public Utilities Board (PUB), Singapore for providing freshwater sludge and relevant information. The funding support provided by National Environment Agency (NEA) (No. USS-IF-2021-1) and Nanyang Technological University, Singapore (No. 04INS000555C120) is appreciated.

Appendix A. Supplementary data

Supplementary data to this article can be found online at https://doi.org/10.1016/j.chemosphere.2021.133298.

References

Babatunde, A.O., Zhao, Y.Q., 2007. Constructive approaches toward water treatment works sludge management: an international review of beneficial reuses. Crit. Rev. Environ. Sci. Technol. 37, 129–164. https://doi.org/10.1080/10643380600776239.
Chen, N., Cao, S., Zhang, Lin, Peng, X., Wang, X., Ai, Z., Zhang, Lizhi, 2021. Structural dependent Cr(VI) adsorption and reduction of biochar: hydrochar versus pyrochar. Sci. Total Environ. 783, 147084. https://doi.org/10.1016/j.scitotenv.2021.147084.
Chowdhury, S., Halder, G., Mandal, T., Sikder, J., 2019. Cetylpyridinium bromide assisted micellar-enhanced ultrafiltration for treating enrofloxacin-laden water. Sci. Total Environ. 687, 10–23. https://doi.org/10.1016/j.scitotenv.2019.06.074.
Chu, D., Ye, Z.L., Chen, S., Xiong, X., 2018. Comparative study of heavy metal residues in struvite products recovered from swine wastewater using fluidised bed and stirred reactors. Water Sci. Technol. 78, 1642–1651. https://doi.org/10.2166/wst.2018.438.
Dassanayake, K.B., Jayasinghe, G.Y., Surapaneni, A., Hetherington, C., 2015. A review on alum sludge reuse with special reference to agricultural applications and future challenges. Waste Manag. 38, 321–335. https://doi.org/10.1016/j.wasman.2014.11.025.
Dong, S., Ji, Q., Wang, Y., Liu, H., Qu, J., 2020. Enhanced phosphate removal using zirconium hydroxide encapsulated in quaternized cellulose. J. Environ. Sci. (China) 89, 102–112. https://doi.org/10.1016/j.jes.2019.10.005.
Fan, H., Liao, J., Abass, O.K., Liu, L., Huang, X., Li, J., Tian, S., Liu, X., Xu, K., Liu, C., 2021. Concomitant management of solid and liquid swine manure via controlled co-composting: towards nutrients enrichment and wastewater recycling. Resour. Conserv. Recycl. 168, 105308. https://doi.org/10.1016/j.resconrec.2020.105308.
Fan, H., Liao, J., Abass, O.K., Liu, L., Huang, X., Wei, L., Li, J., Xie, W., Liu, C., 2019a. Effects of compost characteristics on nutrient retention and simultaneous pollutant immobilization and degradation during co-composting process. Bioresour. Technol. 275, 61–69. https://doi.org/10.1016/j.biortech.2018.12.049.

Fan, H., Liao, J., Abass, O.K., Liu, L., Huang, X., Wei, L., Xie, W., Yu, H., Liu, C., 2019b. Effects of bulking material types on water consumption and pollutant degradation in composting process with controlled addition of different liquid manures. Bioresour. Technol. 288, 121517. https://doi.org/10.1016/j.biortech.2019.121517.

Golet, E.M., Alder, A.C., Giger, W., 2002. Environmental exposure and risk assessment of fluoroquinolone antibacterial agents in wastewater and river water of the Glatt Valley watershed, Switzerland. Environ. Sci. Technol. 36, 3645–3651. https://doi.org/10.1021/es0256212.

Ho, S.H., Chen, Y. di, Yang, Z. kai, Nagarajan, D., Chang, J.S., Ren, N. qi, 2017. High-efficiency removal of lead from wastewater by biochar derived from anaerobic digestion sludge. Bioresour. Technol. https://doi.org/10.1016/j.biortech.2017.08.025.

Jeon, E.K., Ryu, S., Park, S.W., Wang, L., Tsang, D.C.W., Baek, K., 2018. Enhanced adsorption of arsenic onto alum sludge modified by calcination. J. Clean. Prod. 176, 54–62. https://doi.org/10.1016/j.jclepro.2017.12.153.

Karatas, M., 2012. Removal of Pb(II) from water by natural zeolitic tuff: kinetics and thermodynamics. J. Hazard Mater. 199–200, 383–389. https://doi.org/10.1016/J.JHAZMAT.2011.11.035.

Lee, S.Y., Choi, J.W., Song, K.G., Choi, K., Lee, Y.J., Jung, K.W., 2019. Adsorption and mechanistic study for phosphate removal by rice husk-derived biochar functionalized with Mg/Al-calcined layered double hydroxides via co-pyrolysis. Compos. B Eng. https://doi.org/10.1016/j.compositesb.2019.107209.

Li, B., Huang, H., Sun, Z., Zhao, N., Munir, T., Yu, W., Young, B., 2020a. Minimizing heavy metals in recovered struvite from swine wastewater after anaerobic biochemical treatment: reaction mechanisms and pilot test. J. Clean. Prod. 272, 122649. https://doi.org/10.1016/j.jclepro.2020.122649.

Li, J., Li, B., Huang, H., Lv, X., Zhao, N., Guo, G., Zhang, D., 2019. Removal of phosphate from aqueous solution by dolomite-modified biochar derived from urban dewatered sewage sludge. Sci. Total Environ. https://doi.org/10.1016/j.scitotenv.2019.05.400.

Li, R., Wang, J.J., Zhou, B., Awasthi, M.K., Ali, A., Zhang, Z., Lahori, A.H., Mahar, A., 2016. Recovery of phosphate from aqueous solution by magnesium oxide decorated magnetic biochar and its potential as phosphate-based fertilizer substitute. Bioresour. Technol. https://doi.org/10.1016/j.biortech.2016.02.125.

Li, Z., Liu, X., Wang, Y., 2020b. Modification of sludge-based biochar and its application to phosphorus adsorption from aqueous solution. J. Mater. Cycles Waste Manag. 22, 123–132. https://doi.org/10.1007/s10163-019-00921-6.

Liu, Xiaolu, Pang, H., Liu, Xuewei, Li, Q., Zhang, N., Mao, L., Qiu, M., Hu, B., Yang, H., Wang, X., 2021. Orderly porous covalent organic frameworks-based materials: superior adsorbents for pollutants removal from aqueous solutions. Innovations 2, 100076. https://doi.org/10.1016/j.xinn.2021.100076.

Lu, H., Zhang, W., Yang, Y., Huang, X., Wang, S., Qiu, R., 2012. Relative distribution of Pb2+ sorption mechanisms by sludge-derived biochar. Water Res. 46, 854–862. https://doi.org/10.1016/j.watres.2011.11.058.

Mazari, L., Abdessemed, D., Szymczyk, A., 2018. Evaluating reuse of alum sludge as coagulant for tertiary wastewater treatment. J. Environ. Eng. 144, 04018119 https://doi.org/10.1061/(asce)ee.1943-7870.0001462.

Nzediegwu, C., Naeth, M.A., Chang, S.X., 2021. Lead(II) adsorption on microwave-pyrolyzed biochars and hydrochars depends on feedstock type and production temperature. J. Hazard Mater. 412, 125255. https://doi.org/10.1016/j.jhazmat.2021.125255.

Pauletto, P.S., Moreno-Pérez, J., Hernández-Hernández, L.E., Bonilla-Petriciolet, A., Dotto, G.L., Salau, N.P.G., 2021. Novel biochar and hydrochar for the adsorption of 2-nitrophenol from aqueous solutions: an approach using the PVSDM model. Chemosphere 269, 128748. https://doi.org/10.1016/j.chemosphere.2020.128748.

Qu, J., Tian, X., Jiang, Z., Cao, B., Akindolie, M.S., Hu, Q., Feng, C., Feng, Y., Meng, X., Zhang, Y., 2020. Multi-component adsorption of Pb(II), Cd(II) and Ni(II) onto microwave-functionalized cellulose: kinetics, isotherms, thermodynamics, mechanisms and application for electroplating wastewater purification. J. Hazard Mater. 387, 121718. https://doi.org/10.1016/J.JHAZMAT.2019.121718.

Shen, Z., Jin, F., Wang, F., McMillan, O., Al-Tabbaa, A., 2015. Sorption of lead by Salisbury biochar produced from British broadleaf hardwood. Bioresour. Technol. 193, 553–556. https://doi.org/10.1016/j.biortech.2015.06.111.

Shen, Z., Zhang, Y., McMillan, O., Jin, F., Al-Tabbaa, A., 2017. Characteristics and mechanisms of nickel adsorption on biochars produced from wheat straw pellets and rice husk. Environ. Sci. Pollut. Res. 24, 12809–12819. https://doi.org/10.1007/s11356-017-8847-2.

Shen, Z., Zhang, Yunhui, Jin, F., Alessi, D.S., Zhang, Yiyun, Wang, F., McMillan, O., Al-Tabbaa, A., 2018. Comparison of nickel adsorption on biochars produced from mixed softwood and Miscanthus straw. Environ. Sci. Pollut. Res. 25, 14626–14635. https://doi.org/10.1007/s11356-018-1674-2.

Turner, T., Wheeler, R., Stone, A., Oliver, I., 2019. Potential alternative reuse pathways for water treatment residuals: remaining barriers and questions—a review. Water, air. Soil Pollut 230, 227. https://doi.org/10.1007/s11270-019-4272-0.

Wu, Y., Liang, Q., Tang, Q., 2011. Effect of Pb on growth, accumulation and quality component of tea plant. Procedia Eng. 18, 214–219. https://doi.org/10.1016/j.proeng.2011.11.034.

Xu, Z., Xu, J., Yin, H., Jin, W., Li, H., He, Z., 2019. Urban river pollution control in developing countries. Nat. Sustain. 2, 158–160. https://doi.org/10.1038/s41893-019-0249-7.

Zhang, M., Gao, B., Yao, Y., Inyang, M., 2013. Phosphate removal ability of biochar/MgAl-LDH ultra-fine composites prepared by liquid-phase deposition. Chemosphere. https://doi.org/10.1016/j.chemosphere.2013.02.050.

Zhang, X., Zhang, Y., Ngo, H.H., Guo, W., Wen, H., Zhang, D., Li, C., Qi, L., 2020. Characterization and sulfonamide antibiotics adsorption capacity of spent coffee grounds based biochar and hydrochar. Sci. Total Environ. 716, 137015. https://doi.org/10.1016/j.scitotenv.2020.137015.

Zhang, Y., Alessi, D.S., Chen, N., Luo, M., Hao, W., Alam, M.S., Flynn, S.L., Kenney, J.P. L., Konhauser, K.O., Ok, Y.S., Al-Tabbaa, A., 2021a. Lead (Pb) sorption to hydrophobic and hydrophilic zeolites in the presence and absence of MTBE. J. Hazard Mater. 126528 https://doi.org/10.1016/j.jhazmat.2021.126528.

Zhang, Y., Hou, D., O'Connor, D., Shen, Z., Shi, P., Ok, Y.S., Tsang, D.C.W., Wen, Y., Luo, M., 2019. Lead contamination in Chinese surface soils: source identification, spatial-temporal distribution and associated health risks. Crit. Rev. Environ. Sci. Technol. 49, 1386–1423. https://doi.org/10.1080/10643389.2019.1571354.

Zhang, Y., Qin, J., Yi, Y., 2021b. Biochar and hydrochar derived from freshwater sludge: characterization and possible applications. Sci. Total Environ. 763, 144550. https://doi.org/10.1016/j.scitotenv.2020.144550.

Zhang, Y., Wu, L., Huang, P., Shen, Q., Sun, Z., 2018. Determination and application of the solubility product of metal xanthate in mineral flotation and heavy metal removal in wastewater treatment. Miner. Eng. 127, 67–73. https://doi.org/10.1016/J.MINENG.2018.07.016.

Zhao, Y., Li, W., Liu, Z., Liu, J., Zhu, L., Liu, X., Huang, K., 2018. Renewable Tb/Eu-loaded garlic peels for enhanced adsorption of enrofloxacin: kinetics, isotherms, thermodynamics, and mechanism. ACS Sustain. Chem. Eng. 6, 15264–15272. https://doi.org/10.1021/acssuschemeng.8b03739.

Zou, W., Han, R., Chen, Z., Jinghua, Z., Shi, J., 2006. Kinetic study of adsorption of Cu(II) and Pb(II) from aqueous solutions using manganese oxide coated zeolite in batch mode. Colloids Surf. A Physicochem. Eng. Asp. 279, 238–246. https://doi.org/10.1016/j.colsurfa.2006.01.008.